

The Balloon-borne Large Aperture Submillimeter Telescope: BLAST

E. Pascale,¹ P. A. R. Ade,² J. J. Bock,^{3,4} E. L. Chapin,⁵ J. Chung,^{1,5}
 M. J. Devlin,⁶ S. Dicker,⁶ M. Griffin,² J. O. Gundersen,⁷ M. Halpern,⁵
 P. C. Hargrave,² D. H. Hughes,¹² J. Klein,⁶ C. J. MacTavish,¹ G. Marsden,⁵
 P. G. Martin,^{8,14} T. G. Martin,¹ P. Mauskopf,² C. B. Netterfield,^{1,14}
 L. Olmi,^{9,10} G. Patanchon,^{5,13} M. Rex,⁶ D. Scott,⁵ C. Semisch,⁶ N. Thomas,⁷
 M. D. P. Truch,¹¹ C. Tucker,² G. S. Tucker,¹¹ M. P. Viero,¹⁴ D. V. Wiebe¹

ABSTRACT

The Balloon-borne Large Aperture Submillimeter Telescope (BLAST) is a sub-orbital survey-experiment designed to study the evolutionary history and processes of star formation in local galaxies (including the Milky Way) and galaxies at cosmological distances. The BLAST continuum camera, which consists of 270 detectors distributed between 3 arrays, observes simultaneously in broadband (30%) spectral-windows at $250\ \mu\text{m}$, $350\ \mu\text{m}$ and $500\ \mu\text{m}$. The optical design is based on a 2 m diameter Cassegrain telescope, providing a diffraction-limited resolution of $30''$ at $250\ \mu\text{m}$. The gondola pointing system enables raster-like maps of arbitrary geometry, with a repeatable positional accuracy of $\sim 30''$; post-flight pointing reconstruction to $\lesssim 5''$ rms is also achieved. The on-board telescope control software permits autonomous execution of a pre-selected set of maps, with the option of manual intervention. In this paper we describe the primary characteristics and measured in-flight performance of BLAST. Since a test-flight in 2003, BLAST has made two scientifically productive long-duration balloon flights: a 100-hour flight from ESRANGE (Kiruna), Sweden to Victoria Island, northern Canada in June 2005, and a 250-hour, circumpolar-flight from McMurdo Station, Antarctica, in December 2006.

Subject headings: submillimeter — galaxies: evolution — stars: formation — instrumentation: miscellaneous — balloons

¹Department of Physics, University of Toronto,
 60 St. George Street, Toronto, ON M5S 1A7,

Canada; enzo@physics.utoronto.ca

²Department of Physics & Astronomy, Cardiff

1. Introduction

We have built and flown a balloon borne submillimeter observatory, designed to study the star formation in our Galaxy and in high redshift starburst galaxies by exploiting a window at several hundred microns which is not useable from the ground.

The Balloon-borne, Large Aperture, Submillimeter Telescope (BLAST) is a stratospheric balloon-borne 2 m telescope which observes the sky with bolometric detectors operating in three bands at $250\ \mu\text{m}$,

$350\ \mu\text{m}$, and $500\ \mu\text{m}$. The diffraction-limited optics are designed to provide BLAST with a resolution of $30''$, $42''$, and $60''$, respectively. The detectors and cold optics are adapted from those to be used on the SPIRE instrument on *Herschel* (Griffin et al. 2003). By providing the first sensitive large-area ($\sim 0.8 - 200\ \text{deg}^2$) submillimeter surveys at these wavelengths, BLAST addresses important Galactic and cosmological questions regarding the formation and evolution of stars, galaxies and clusters (Devlin et al. 2004).

Taking advantage of the unique spectral-coverage, resolution and sensitivity, the primary scientific goals of BLAST are to i) conduct confusion-limited and shallower wide-area extragalactic surveys to constrain the redshift-distribution, star formation history and evolution of optically-obscured luminous galaxies, by measuring robust photometric-redshifts (derived from the BLAST colors, and complementary data, Hughes et al. 2002), and the spatial clustering of this population; ii) to improve our understanding of the earliest stages of star formation by determining the physical properties and mass-function of cold pre-stellar cores, and the efficiency of star formation within different Galactic environments; and iii) to investigate the nature and structure of the interstellar medium by making high resolution maps of diffuse Galactic emission.

BLAST had a 24 hours test flight (BLAST03) from Fort Sumner, NM, in September 2003, which demonstrated the performance of the instrument sub-systems.

BLAST made its first science flight (BLAST05) in June of 2005, flying on a $1.1 \times 10^6\ \text{m}^3$ balloon from the Swedish

University, 5 The Parade, Cardiff, CF24 3AA, UK

³Jet Propulsion Laboratory, Pasadena, CA 91109-8099

⁴Observational Cosmology, MS 59-33, California Institute of Technology, Pasadena, CA 91125

⁵Department of Physics & Astronomy, University of British Columbia, 6224 Agricultural Road, Vancouver, BC V6T 1Z1, Canada

⁶Department of Physics and Astronomy, University of Pennsylvania, 209 South 33rd Street, Philadelphia, PA 19104

⁷Department of Physics, University of Miami, 1320 Campo Sano Drive, Coral Gables, FL 33146

⁸Canadian Institute for Theoretical Astrophysics, University of Toronto, 60 St. George Street, Toronto, ON M5S 3H8, Canada

⁹Istituto di Radioastronomia, Largo E. Fermi 5, I-50125, Firenze, Italy

¹⁰University of Puerto Rico, Rio Piedras Campus, Physics Dept., Box 23343, UPR station, San Juan, Puerto Rico

¹¹Department of Physics, Brown University, 182 Hope Street, Providence, RI 02912

¹²Instituto Nacional de Astrofísica Óptica y Electrónica (INAOE), Aptdo. Postal 51 y 72000 Puebla, Mexico

¹³Laboratoire APC, 10, rue Alice Domon et Léonie Duquet 75205 Paris, France

¹⁴Department of Astronomy & Astrophysics, University of Toronto, 50 St. George Street, Toronto, ON M5S 3H4, Canada

Space Corporation base of ESRANGE, near Kiruna, Sweden to Victoria Island in northern Canada. During this 4.5 day flight at an average altitude of 38 km, the instrument performed well, except for degraded optical performance. This was possibly due to a failure of structural elements in the carbon fiber mirror, and resulted in decreased resolution, which had a significant impact on our ability to achieve our extragalactic science goals. BLAST acquired 100 hours of data on Galactic targets, providing some of the first arcminute resolution images at these wavelengths. In this flight, surveys were conducted of five star forming regions, including the well-studied Cygnus-X field, three regions of intermediate/high-velocity cirrus, the Cas-A supernova remnant, and several individual bright targets.

BLAST made its second science flight (BLAST06) in December, 2006, flying from the Williams Field Long Duration Balloon (LDB) facility near McMurdo Station in Antarctica. In this flight the instrument met its performance goals in resolution, sensitivity, and pointing. The flight was terminated after 250 hours of data were acquired. Unfortunately, an anomaly with the parachute separation system prevented the parachute from being released from the gondola after landing. The parachute dragged BLAST for 250 km before it came to rest in a crevasse field on the Antarctic Plateau. While most of the instrument was destroyed, the hard drives containing the data were found nearby, and the complete dataset recovered. In this flight, BLAST conducted shallow (10 deg^2) and deep, confusion-limited (0.8 deg^2) extragalactic surveys of the CDF-S as well

as a 10 deg^2 region near the south ecliptic pole. A Galactic survey in Vela mapped 52 deg^2 and 200 deg^2 of sky in deep and shallow observations, respectively. Surveys of several Galactic and extragalactic selected targets were also conducted.

A brief overview of BLAST science, in the context of current and future Far Infrared (FIR) and submillimetric experiments, is given in Section 2. The telescope and optics are described in Section 3, while Sections 4 and 5 focus on detector arrays and cryogenics. Sections 6 to 8 provide detailed information regarding the gondola, command and control, and pointing systems. Sections 9 to 12 provide overviews of the unique thermal and power requirements, and a description of the pointing performance.

2. BLAST in the context of other FIR-submillimeter experiments

The BLAST bands bracket the peak of the thermal radiation emitted by dust at temperatures of around 10 K. Assuming that the temperature range of dust in submillimeter galaxies is $\sim 30 - 60 \text{ K}$, BLAST can explore redshifts from 1 to 5 (Hughes et al. 2002). The primary advantage of BLAST over existing submillimeter bolometer arrays such as SCUBA and SHARC is its greatly enhanced sensitivity at wavelengths $\leq 500 \mu\text{m}$, due to the dramatically increased atmospheric transmission at balloon altitudes. With proposed sensitivities of $250 \text{ mJy s}^{1/2}$, the BLAST mapping speed is 10 times faster than the design goal for SCUBA 2 at $500 \mu\text{m}$ (Holland et al. 2006), and more than 100 times the mapping speed of the pioneering flights of the

FIR balloon-borne telescope PRONAOS (Lamarre et al. 1998). BLAST is complemented at shorter wavelengths by surveys from *IRAS*, *ISO*, *Spitzer*, *Akari*, and at longer wavelengths by SCUBA 2, LMT, and ALMA, to constrain spectral energy distributions. *Spitzer*'s higher resolution also provides accurate astrometry for many of the BLAST sources. BLAST complements the *Herschel* satellite by testing detectors and filters which are similar to those to be used in the SPIRE instrument (Griffin et al. 2003). Furthermore, the results from BLAST will be available early enough to influence the design (depth and area) of future SPIRE surveys. In addition, BLAST will complement the large-area spectroscopic Galactic surveys of *SWAS*, provide submillimeter targets for the Fabry-Perot spectrograph SAFIRE on *SOFIA*, and impact the design of the scientific case for the next generation of submillimeter surveys from space (e.g. *SPICA* and *SAFIR*, and later *SPIRIT* and *SPECS*).

3. Telescope

The basic BLAST optical configuration is shown in Figure 1. Incoming radiation is collected by a Cassegrain telescope (M1 and M2 in the figure) which is located on the inner frame of the gondola (described in Section 6), along with the cryogenic receiver (Section 5). The Cassegrain focus is located about 20 cm behind the optical surface of the primary. Cold (1.5 K) re-imaging optics (M3, M4, and M5) in the receiver relay the sky image to the detector focal planes. A baffled Lyot stop (M4) is located at the position of an image of the primary mirror. This blocks stray

radiation due to scattering and diffraction. After M5 the radiation is divided into three spectral bands through the use of two low-pass edge dichroic filters (Ade et al. 2006). An aperture at the center of the Lyot stop is made to match the one at the center of the primary mirror to reduce loading. This same hole accommodates a commandable thermal source, which provides a stable and repeatable optical signal (calibration lamp) to monitor detector responsivity drifts (Hargrave et al. 2006). The optical design is optimized to deliver a diffraction-limited image of the sky at the detector focal planes, with 60'' and 30'' beams at 500 μm and 250 μm , respectively. The telescope design of BLAST05 and BLAST06 is discussed later in this section and the relevant parameters can be found in Table 1.

3.1. Focal Plane

The illumination of the Lyot stop and the main reflector depends primarily on the properties of the feed-horns in the detector array. BLAST uses $2f\lambda$ spaced, smooth-walled conical feeds which are similar to SPIRE feeds. Their design and measured characteristics have been described by Chattopadhyay et al. (2003), Rownd et al. (2003), and Griffin et al. (2002). The optical system design is based upon the feed-horn nominal $f/5$ focal ratio and requires the chief-rays to be perpendicular to the aperture of the horn, with all the beams overlapping at the Lyot stop. Knowledge of the fundamental propagated electromagnetic mode (TE_{11}) is used in a Zemax¹ Physical Optics module to verify

¹<http://www.zemax.com/>

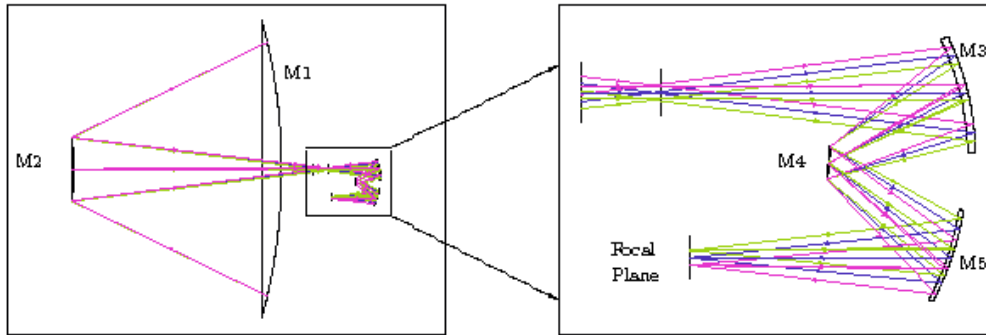


Fig. 1.— The optical layout of the BLAST05 telescope and receiver is shown on the left and the 1.5K optics which are located within a cryostat are shown expanded on the right. The image of the sky formed at the input aperture is re-imaged onto the bolometer detector array at the focal plane. The mirror M4 serves as a Lyot stop defining the illumination of the primary mirror for each element of the bolometer array. The three wavelength bands are defined by a pair of dichroic beamsplitters (not shown) which are located between M5 and the focal plane.

the final design.

3.2. BLAST05 Optical Design

For the 2005 flight, the design incorporated a 2 m carbon-fiber spherical primary mirror with a mass of 32 kg and a surface rms of $2.4 \mu\text{m}$. It was designed and built by Composite Optics Incorporated² as a technology prototype for the 3.5 m *Herschel* telescope. An aluminum correcting secondary mirror, with a diameter of 50 cm, gave diffraction-limited performance over a $14' \times 7'$ field of view (FOV) at the Cassegrain focus. The estimated antenna efficiency was $\geq 80\%$; losses came from a combination of the rms surface roughness of the primary and the quality of the re-imaging optics. Two of the re-imaging cold elements, M3 and M5, are ellipsoidal mirrors; M2 and the other

cold element, M4, compensate for most of the spherical aberration of the primary, whereas M3 and M5 contribute to achieve the correct focal ratio. The perimeter of the primary mirror was structurally weak, forcing M2 to be suspended by a carbon-fiber structure, attached through the hole in the primary mirror. This geometry resulted in $\sim 12\%$ blockage of the beam, leading to significant projected loading on the detectors for all three bands. Although various optical solutions for ground visible/IR telescopes using a spherical primary are discussed in the literature, in our case, peculiar design constraints had to be respected (mainly weight and size). A full discussion can be found in Olmi (2001, 2002), where the optimization procedure and the basic optical configuration are also discussed. The 2 m primary mirror was under-illuminated by setting the entrance pupil diameter to 188 cm, and the reflector was strongly tapered, resulting in a

²Composite Optics Incorporated (COI), 9617 Distribution Avenue, San Diego, CA 92121.

field taper of about -15 dB. A Strehl ratio > 0.96 was achieved over the whole focal plane, and far field beams had a first side-lobe at -10 dB. A detailed analysis of the relation between Strehl ratio and aperture efficiency, which is more commonly quoted for filled-aperture antennas, can be found in Olmi (2007).

3.3. BLAST06 Optical Design

In the 2006 Antarctic flight, BLAST flew a Ritchey-Chrétien telescope, with a 1.8 m diameter, aluminum primary mirror with a mass of 114 kg. Originally, the mirror was intended to be used only for the test flight in 2003. However, after the destruction of the carbon fiber mirror on landing of BLAST05, the aluminum mirror was re-machined to improve the quality of the surface from $8 \mu\text{m}$ to better than $4 \mu\text{m}$ rms. This machining was performed by the Precision Engineering Group at Lawrence Livermore National Laboratory. A 40 cm diameter aluminum secondary was suspended by four carbon fiber struts³ (with a zero linear thermal expansion coefficient) attached to the perimeter of the primary mirror, which reduced the obscuration to $\sim 7\%$. The loading on the detectors was reduced further with the installation of angled reflecting baffles under each strut to deflect most of the obscured beam to the relatively cold sky. The cold re-imaging optics form an ideal Offner relay. In this configuration, M3, M4, and M5 are all spherical and share a common center of curvature; M3 and M5 are concave while M4 is convex. In order to achieve a

³ Innovative Composite Engineering, 139 E. Columbia River Way, Bingen, WA 98605.

diffraction-limited beam of $60''$ at $500 \mu\text{m}$ and $30''$ at $250 \mu\text{m}$ with a smaller diameter primary compared to BLAST05, M1 was more aggressively illuminated. This was made possible by reducing the diameter of the Lyot stop by about 12%, leading to a field taper of -7.5 dB on M1 and -17 dB sidelobes in the far field beams.

3.4. BLAST06 Focussing System

The relative distance between the primary and the secondary mirrors has a tolerance of one λ before significant image degradation is introduced. Thermal modeling indicated that diurnal temperature fluctuations at balloon altitudes of the aluminum M1 and M2 mirrors could have been as large as 10°C . The required correction in the relative distance between M1 and M2 was calculated to be $50 \mu\text{m}/^\circ\text{C}$.

To correct for this, we implemented a motorized system for in-flight refocussing of the secondary. M2 was coupled to its mounting structure via 17-7PH stainless steel leaf springs. Three stepper motor actuators⁴ (2.12 mm rev^{-1} lead screw) drive the mirror back and forth to correct for the focus position, as well as adding tip/tilt capability to initially align M2 to M1. Accurate positioning was achieved with differential optical encoders ($\simeq 1 \text{ count } \mu\text{m}^{-1}$ resolution) factory mounted to the motors, and three DC Linear Variable Differential Transformers⁵ (LVDT). This system allowed for ± 5 mm of motion about the nominal telescope focus, which was sufficient

⁴Ultra Motion, 22355 Route 48, #21, Cutchogue, NY 11935.

⁵Macro Sensors, 7300 US Route 130 North, Building 22, Pennsauken, NJ 08110, $0.6 \mu\text{m}$ or better repeatability.

for accurate positioning. The flight computer commands each motor individually by communicating with the stepper motor controllers over a RS485 bus.

Pre-flight focussing of the system was hampered by the fact that water vapor absorption makes ground-based submillimeter observations in the far-field of the telescope (about 10 km) impossible. To mitigate this, the secondary mirror was physically offset to 3 positions so that the focal plane was reimaged at 50, 100, and 150 m from the telescope. The focussing system was then used to fine-tune the focus at each position. These results were extrapolated to determine the far-field focus for the flight.

In flight, the focus of the system was verified and had to be manually adjusted by maximizing the response when scanning over bright point sources: a correction of 300 μm to the position set at launch was found required. Subsequently, the temperatures of the primary and secondary were monitored and the secondary automatically repositioned to account for thermal variations that would produce a focus displacement of 100 μm or more. In flight, the primary and secondary mirror diurnal temperature fluctuations were $\pm 1.5^\circ\text{C}$ for most of the flight.

3.5. Array Bandpass Characteristics

Low-pass edge dichroic filters (Ade et al. 2006) split the incoming radiation emerging from M5. The first dichroic reflects wavelengths shorter than 300 μm and transmits longer wavelengths. The bandpass for the 250 μm array is further defined by a filter directly in front of the

array, which reflects wavelengths shorter than 215 μm , and by the waveguide cutoff at the exit of each of the feedhorns. For the 350 μm array, the band is defined at the short wavelength end by the transmission of the first dichroic and at the long wavelength end by the waveguide cutoff. The 500 μm band is defined at the short wavelength end by the transmitted radiation from the second dichroic and at the long wavelength end by the feedhorn cutoff. Each band has a 30% width. The filter stack frequency performance was evaluated with Fourier Transform Spectroscopy. Bandpasses are shown in Figure 2.

4. Receiver

The BLAST focal plane consists of arrays of 149, 88, and 43 detectors at 250 μm , 350 μm , and 500 μm , respectively. The arrays are cooled to a temperature of 300 mK. Each array element is a silicon nitride micromesh “spider web” bolometer (Bock et al. 1996). The detector arrays, the feeds, and the mounting scheme are based on the SPIRE instrument design (Turner et al. 2001). Each array hosts a number of diagnostic channels: two dark bolometers (channels that have been capped to avoid illumination), two thermistor, and one resistor. The detector parameters are summarized in Table 2.

Each bolometer consists of a photolithographed mesh that provides high absorption efficiency over a wide frequency range, as well as providing low heat capacity (Turner et al. 2001). An additional advantage to this design is the relatively small cross-section to cosmic rays. Balloon flights at high-latitudes have about 100 times the mid-latitude cosmic ray flux. A

Neutron Transmutation Doped (NTD) germanium thermistor glued to the absorber measures the bolometer temperature and therefore the flux of incoming photons.

The detectors and the readout electronics are designed so that the sensitivity is ultimately limited by the photon “BLIP” noise. To achieve this performance, other contributions to the bolometer noise have to be controlled. A bolometer is fundamentally limited by phonon noise in the thermal link with the heat sink. The Noise Equivalent Power (NEP) is in this case $NEP = \gamma \sqrt{4k_{\text{B}}T^2G}$, where G is the thermal conductance, T is the bath temperature and γ takes into account the Johnson noise in the thermistor. For a given background load Q , the maximum sensitivity is achieved when $G \sim Q/T$ (Mather 1984). The detectors have been optimized for loads of 55, 40 and 30 pW at 250 μm , 350 μm , and 500 μm , respectively. The detector transfer function is measured using cosmic ray hits, as described in Crill et al. (2003), and we have found typical time constants of ~ 2 ms.

4.1. Readout Electronics

A schematic diagram of the readout electronics is shown in Figure 3. Each bolometer is pre-amplified with a Siliconix U401 differential JFET with 5–7 nV Hz^{-1/2} noise at $\nu > 100$ Hz. Compact 24 channel JFET modules are integrated into the design of the cryostat, allowing us to sink their power dissipation (240 μW per pair) to the vapor-cooled shield (see Section 5) and decrease the load on the helium bath by approximately 60 mW. The JFET are operated at a temperature of ~ 145 K. Their output is then amplified using the

Analog AD624 instrumentation amplifier (5 nV Hz^{-1/2}) with a 100 Hz wide band-pass filter, centered at 208 Hz. To mitigate the effects of $1/f$ noise, the detectors are AC biased with a sine wave at 200.32 Hz. A reference square wave at this frequency is generated by dividing down the main 32 MHz clock serving the readout electronics, making the bias synchronous with the sampling. This signal is then split into three paths (one per band), stabilized to a voltage amplitude that is selectable from 0 to 300 mV with a resolution of 7 bits, and filtered into a sine wave using low-noise operational amplifiers (Analog OP470). The bias is delivered to the detectors and a reference is sent back to the Data Acquisition System (DAS) where a digital lock-in is implemented on the DSP (Analog ADSP21062) in the readout electronics. The bolometric AC signals and the bias reference are digitized with a 24 bit $\Sigma\Delta$ (Burr-Brown ADS1252) fed by a low-noise dual instrumental amplifier (Burr-Brown INA2128) and sampled at 10 kHz. The reference is phase-locked and a numerical sine wave is generated in-phase at the bias frequency (the clock is shared). The rectified signal is then low-passes with a 4 stage boxcar filter having a first null at 50.08 Hz, and decimated to match the DAS sampling frequency (100.16 Hz).

The resulting flat-phase filter is well approximated by a Gaussian and is computationally efficient in the time domain, allowing up to 25 independent channels to be locked-in on a single DSP. Only the real part of the signal is sampled, hence the relative phase between signal and reference must be manually set. Since the phase difference is a function of the bolometer

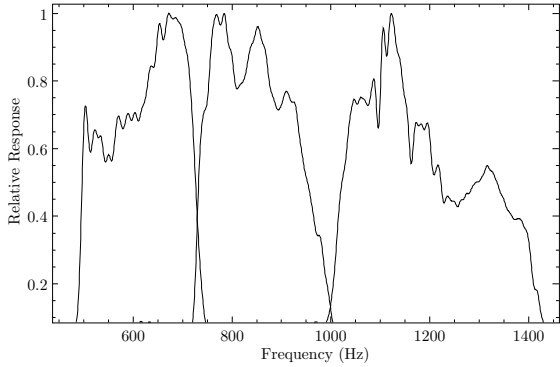


Fig. 2.— Relative spectral response of the three BLAST channels for a flat-spectrum source, measured during the BLAST06 campaign. The peak response in each band has been normalized to one. Absorption from residual water vapor inside the Fourier transform spectrometer is visible in all the bands.

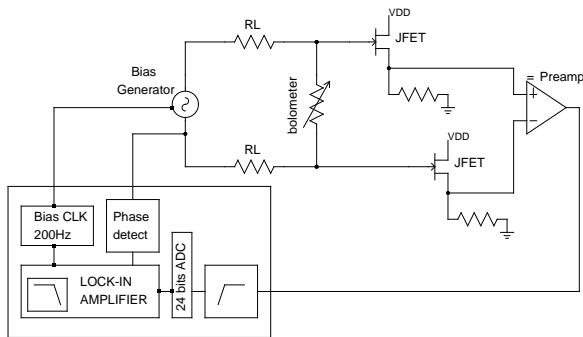


Fig. 3.— A schematic diagram of the detector readout electronics. A 200.32 Hz sine wave biases each bolometer across two 7 M Ω load resistors. JFET pairs buffer the detector signal to the warm electronics. The two signals are then differenced and digitized. A digital lock-in rectifies and filters the output sending it to the flight computers over the BLASTbus.

impedance, it needs to be adjusted in flight along with bias levels. This is achieved by maximizing the signal from the pulsed calibration lamp at the Lyot stop.

The overall data acquisition electronics noise is kept below the estimated photon noise and provides stability to low frequencies (< 30 mHz), which allows the sky to be observed in a slowly-scanned mode.

4.2. Detector Noise

The voltage noise is determined by taking the power spectral density of a deglitched time stream acquired in flight. The electronic time constant is then deconvolved and common-mode signals are removed as described by Patanchon et al. (2007). The final average noise is plotted in Figure 4 as a function of frequency for a representative detector.

5. Cryogenics

The cryostat houses most of the receiver system (Figure 5) and was fabricated by Precision Cryogenics⁶. It is constructed of aluminum, for its strength to weight ratio, and G10 woven fiberglass reinforced resin epoxy when minimal thermal conduction is required. The cryostat is maintained at vacuum to prevent thermal convection, and each thermal stage fully encloses the next colder stage to reduce radiative thermal loading, except for the optical path, which is thermally protected with infrared blocking filters. Super-insulation, consisting of twenty layers of aluminized Mylar, is used to further reduce the emissivity of the aluminum and G10, and therefore the radiative load.

⁶<http://www.precisioncryo.com/>

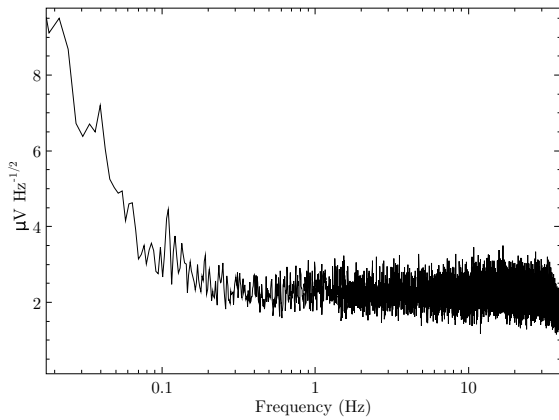


Fig. 4.— A $250\ \mu\text{m}$ detector noise power spectrum density, acquired during the BLAST05 flight with the telescope scanning one extragalactic target. Common modes are corrected as described by Patanchon et al. (2007). The telescope fundamental scan frequency is visible at $\sim 0.04\ \text{Hz}$ as well as its first odd harmonic at $\sim 0.12\ \text{Hz}$. Detectors at different colors have similar performance. The BLAST05 calibration can be found in Truch et al. (2007).

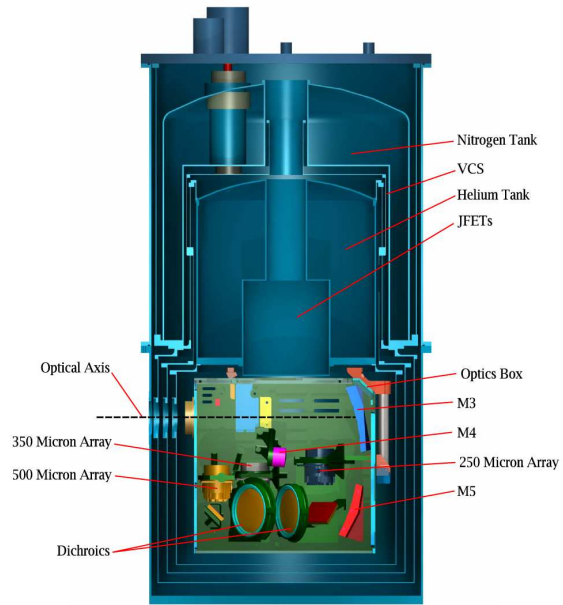


Fig. 5.— Cutaway drawing of the BLAST receiver showing the optics box. The ^3He refrigerator is omitted for clarity. The cryostat is held to the telescope structure via bolts in the top flange and jack screws around the perimeter near the base.

Liquid baths of nitrogen and helium maintain the temperatures of the 77 K and 4.2 K stages. In flight, an absolute pressure regulator⁷ is used to maintain approximately 1 atm above each bath. Tests were performed to verify the pressure regulator would not introduce flutter causing vibrations or temperature oscillations. A vapor-cooled shield (VCS) is located between the nitrogen and helium stages. Boil-off gas from the helium bath passes through a heat exchanger in thermal contact with the VCS before venting out of the cryostat. The VCS reduces the thermal loading on the helium stage and therefore increases the hold-time. Simulations of the cryostat with TAK 2000 Lite⁸ thermal analysis software were used during the design process to ensure long-duration (> 11 day) hold time with a minimum weight and size. Radiative and conductive loading is 7.2 W on the nitrogen tank and 71 mW on the helium tank. An additional effective load of 9 mW and 7 mW on the helium tank is due to the liquid drawn into the pumped-pot by the capillary (discussed below), and heating required to cycle the ^3He refrigerator, respectively. The cryostat holds 43 L of nitrogen and 32 L of helium.

A liquid He pumped-pot maintains the optics box at 1.5 K. A long, thin capillary connects the helium bath to the pumped-pot with a volume of ~ 100 mL. A pump line between the pot and the exterior of the cryostat keeps the pot at near vacuum, maintaining the temperature at 1.5 K. The pressure difference between the helium bath and the pot forces helium into the pot; the length and diameter of the cap-

illary are tuned to provide the minimum amount of helium to keep the pot cold. On the ground, a vacuum pump is used; at float altitude, the pump line is open to the atmosphere, which is at a pressure < 0.01 atm.

The bolometers and feed horns are maintained at < 300 mK by the closed-cycle ^3He refrigerator. The ^3He is condensed by the 1.5 K pumped-pot, and collects in the ^3He cold stage. Once all the ^3He has condensed, a charcoal sorption pump lowers the pressure above the ^3He , bringing the temperature below 300 mK. When the liquid ^3He is exhausted, the charcoal is heated to > 20 K, and the ^3He is released to be condensed by the pumped-pot and the cycle repeats. During a cycle, the added heat load on the helium tank increases the boil-off and therefore further cools the VCS. The ^3He refrigerator is able to extract 5 J of energy, and needs to be recycled every 48–60 hours. Each cycle takes less than 2.5 hours.

The cryostat performed as expected during both science flights. The nitrogen and helium baths maintained constant temperature, and the VCS fluctuated by less than 3 K due to the ^3He refrigerator cycles. The pumped-pot maintained a temperature below 1.8 K with fluctuations less than 10 mK. During ^3He refrigerator cycles the pumped-pot temperature rose as high as 2.5 K. The bolometer temperature was maintained below 300 mK with less than 1 mK fluctuations on hour time scales. The first science flight was too short to test hold time. In the second 12.5 day flight, the helium tank was exhausted 11.5 days after reaching float altitude. The nitrogen tank was not exhausted before ter-

⁷Tavco, Inc, 20500 Prairie St., Chatsworth, CA.

⁸<http://www.tak2000.com/>

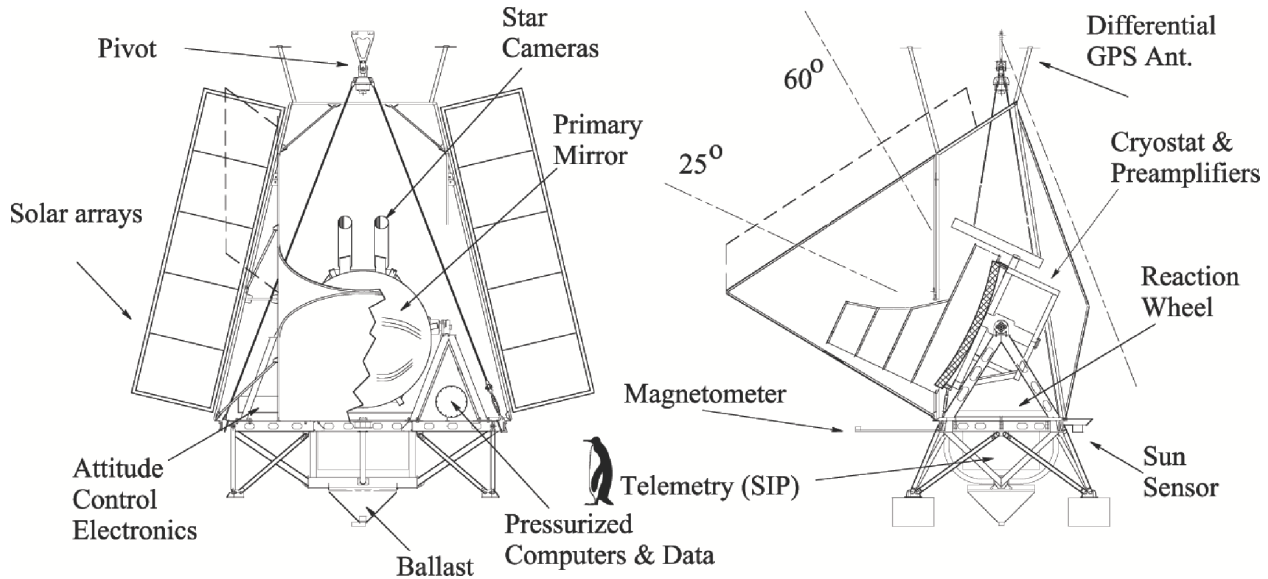


Fig. 6.— Front and side schematic drawings of the BLAST gondola. A 1 m tall Emperor penguin is shown for scale. The height of the pivot is set by the size of the launch vehicle and the width of the gondola *without* deploying the solar panel arrays matches the width of the laboratory doors. The inner frame, which can be pointed in elevation, consists of the two star cameras, the telescope and its light baffle, the receiver cryostat and associated electronics. The telescope baffle shown at right, which was used in 2005, was replaced by a smaller system in 2006. The CSBF solar panels and transmitting antennae are suspended below the structure shown here. The lines marked 25° and 60° show the useful range of orientation of the optic axis. The dot-dashed line at the right originating above the pivot shows a 20° avoidance zone required to avoid accidental contact at launch. The dashed parallelogram at the top in the right hand diagram, and to the left in the left hand diagram shows the shape of an extension to the sun shields added for the Antarctic flight to allow observations to be made further from the anti-sun direction.

mination.

6. Gondola

The BLAST gondola provides a pointed platform for the telescope and the attachment point to the balloon flight train. The gondola was designed and built by AMEC Dynamic Structures⁹, based on initial designs from members of the BLAST team. Schematics of the gondola are shown in Figures 6 and 7. The breakdown of the mass of various components is given in Table 3.

6.1. Requirements

The gondola design is driven by the stringent pointing requirements of the science-case. The elevation range of the inner frame, including the 2 m primary mirror and the ~ 200 kg cryostat, is $25 - 60^\circ$. The entire gondola can rotate to any azimuth angle. The in-flight pointing is accurate to $\sim 30''$ and post-flight pointing reconstruction is accurate to better than $5''$. The telescope's primary observing mode is to scan in azimuth at $\sim 0.1^\circ \text{ s}^{-1}$. Finally, the mirrors are shaded from solar radiation.

As a consequence of the pointing requirements, the feedback rate of the control system is ~ 10 Hz. To accommodate this, the gondola is designed to be rigid, with a minimum resonance frequency greater than 14.4 Hz. All mechanical tolerances are set to minimize backlash. All bearings are low friction and low stiction with low-temperature grease. The center-of-mass of the system is on the rotational

axis so that translations of the gondola (by wind or from the balloon) do not generate torques which re-orient the telescope.

A target weight of ~ 2000 kg was set for the entire system. The maximum width and height of the gondola are constrained by the geometry of the buildings in the field where the gondola is assembled. The launch procedure requires that, in the launch orientation, no part of the gondola intersects a plane 20° from vertical passing through the launch vehicle/gondola attachment point. A final constraint on geometry is that all components of the gondola must fit into standard sea shipping containers. Additionally, the gondola must survive the vibrations and shocks suffered during launch and there must be no structural failure during any of the possible load cases under parachute shock, that can be as high as 10 g along the vertical. Finally, the mechanical tolerances must account for temperatures which vary by as much as $\sim 100^\circ \text{ C}$ during the course of the flight.

6.2. Layout

The gondola frame consists of three components: an outer frame, suspended from the balloon flight train by cables and a pivot motor; an inner frame which is attached to the outer frame at two points along a horizontal axis; and a set of Sun shields that attach to the outer frame. The frame is mostly constructed of light-weight aluminum tubing and I-beams. BLAST incorporates large-diameter torque motors for all motion control.

⁹<http://www.amecds.com/>

6.2.1. Major Components

The outer frame consists of a horizontal surface, 2 yokes to support the inner frame, and four legs. The outer frame is pointed in azimuth using a reaction wheel and pivot. It also provides mounts for various electronics boxes, including the flight computers, the Columbia Scientific Balloon Facility (CSBF) electronics, various pointing sensors, and flight batteries.

The inner frame is made from thin-wall aluminum box beam. It supports the telescope, cryostat, detector read-out electronics, gyroscopes and star cameras. It is attached to the outer frame at two points, defining an axis of rotation.

The back, sides and bottom of the gondola are surrounded by Sun shields, allowing the telescope to point as low as 25° in elevation. A lightweight aluminum frame encloses the telescope and is covered with extruded polystyrene panels wrapped in aluminized Mylar. The original design shielded the secondary mirror from the Sun at 30° above the horizon, the highest the Sun rises during an Antarctic flight, with the telescope pointing directly away from the Sun. Additional panels were added for the BLAST06 flight to improve the shading when the telescope is not pointed anti-Sun. The telescope is also protected from solar radiation scattered from the ground. As well as the opening for the telescope, there are forward-facing openings in the Sun shields to allow for cooling of the electronics by radiation (see Figure 7).

6.2.2. Attitude Control

The telescope's attitude is controlled by three torque motors: the reaction wheel,

pivot and elevation motors. The motors are rare-earth, permanent-magnet, direct-drive DC torque motors¹⁰ with a peak torque of 13.6 Nm. They are controlled by 50 A pulse-width modulated servo amplifiers.¹¹ The housings, made of hardened steel, are custom designed and incorporate the bearings. The original design called for a dry Teflon bearing lubricant, but we found that low-temperature bearing grease¹² provides lower friction and stiction.

The telescope is controlled in azimuth by a 1.5 m reaction wheel, made of 7.6 cm thick aluminum honeycomb, and forty-eight, 0.9 kg brass disks mounted around the perimeter to maximize the ratio of moment of inertia to mass. The reaction wheel is mounted on the outer frame, at the center of the platform, with its rotation axis going through the pivot. Torquing the gondola against the reaction wheel controls azimuth pointing.

The gondola is subject to external torque from wind shear acting on the gondola and from balloon rotation acting through the flight train. The second term is minimized, but not entirely eliminated, by installing a vertical axis pivot at the attachment of the gondola to the flight train. See Figure 6. Torque motors can not run at high rotational speeds, and the reaction wheel motor might saturate while trying to overcome these torques, so an additional torque motor placed in the pivot is used to reduce excess angular momentum and keep the rotation of the reaction wheel within

¹⁰Koll Morgen QT-6205.

¹¹Advanced Motion Controls, model 12A8K.

¹²Dow Corning Molykote[®] 33.

reasonable limits. Figure 8 demonstrates that this nested servo system, where the reaction wheel is driven to maintain telescope orientation and the pivot is driven to maintain low reaction wheel speed, successfully decouples the telescope from external torques.

The elevation of the inner frame is controlled by a motor mounted on one side of the inner frame, at the attachment point to the outer frame. A free bearing provides the connection point on the other side. The motor housing incorporates a 16-bit shaft encoder¹³ which measures the orientation of the inner frame relative to the outer frame. A fluid transfer system, consisting of a pump and two tanks containing ~ 10 L of a high-density non-toxic fluid¹⁴, corrects for long time-scale balance offsets induced by the boil-off of the cryogenics.

The balloon environment introduces small oscillations in pitch and roll of the gondola. A roll damping system consisting of a motor and a small 30 cm diameter reaction wheel is mounted perpendicular to the flywheel on the outer frame. Oscillations in pitch are removed by controlling the elevation of the inner frame.

7. Command and Control

The BLAST observatory is designed to operate autonomously, without need of ground commanding. Telescope control is provided by a pair of redundant flight computers with Intel Celeron processors at 366 and 850 MHz, running Slackware¹⁵ Linux 9.2 with 2.6.8 Kernel. The computers are

kept at near atmospheric pressure to allow the hard drives to function properly, and to provide the appropriate thermal environment for the CPUs.

7.1. Telemetry

The communication link between the telescope and the ground is provided by CSBF through a number of line-of-sight (LOS) transmitters and satellite links. The LOS data-link is available while the payload is in line-of-sight of a receiving station, usually the first part of the flight; satellite link is available for the whole duration of the flight. On board, the interface between the flight computer and telemetry is provided by CSBF's Support Instrumentation Package (SIP). The ground station computers interface with CSBF's ground station equipment to send commands to the payload and display down-linked data. The ground station software uses `kst`¹⁶ and other Linux applications developed by BLAST team members.

7.2. Gondola Electronics

The flight computers are built upon a passive PCI-bus backplane and contain a single board computer, a four port 8250 serial port extender card, and a custom made PCI controller card, which interfaces major components as well as the LOS data transmitter. This card interfaces with the BLASTbus, a proprietary RS485 bus with three differential pairs (data, clock, strobe). The BLASTbus protocol is a poll and response architecture composed of a 32-bit request followed by a 32-bit response

¹³Gurley Precision Instruments A25SB.

¹⁴Dynalene HC-40.

¹⁵<http://www.slackware.com/>

¹⁶<http://kst.kde.org/>

containing 16 bits of data. The BLASTbus clock runs at 4 MHz, giving an effective bandwidth on the BLASTbus of 1 Mbit/s.

The BLASTbus connects the flight computers to the Attitude Control System (ACS) and DAS. Each DSP card in these systems monitors the BLASTbus. They provide data upon request, and receive command input from the flight computers via the BLASTbus.

Data are marshalled on the BLASTbus into 100 Hz frames. Bolometers are polled once per frame, as are the gyroscopes and other high-precision pointing data. The majority of housekeeping signals do not need to be polled at 100 Hz. These “slow data” signals are polled at 5 Hz with groups of twenty multiplexed into a single 100 Hz channel. The 100 Hz frames provide the basic data structure for data archival. The frames are written to disk and transmitted by the line-of-sight 1 Mbit/s transmitter.

In addition to the BLASTbus, the flight computers also collect data via 8250-style serial connections to the differential GPS, the SIP computers, the lock motor, and the secondary actuators. Ethernet provides further connectivity to the star camera computers and Sun sensor computer. Data collected on the auxiliary channels is written back to the BLASTbus in order to synchronize these data with the 100 Hz frame clock. The star cameras are triggered via the BLASTbus to provide data synchronization.

7.3. Flight Software

The flight computers run a single, monolithic program, the “master control program” (mcp), written in C, which per-

forms primary control of all aspects of the telescope including in-flight pointing solution, motion, commanding, telemetry, data archiving, and thermal control.

7.4. Pointing Control

BLAST is a scanning experiment. The primary scan-mode involves an azimuthal raster coupled with a slow elevation drift or discrete elevation steps.

Detector response times, τ , together with $1/f$ noise, and star camera integration times set limits on the azimuthal scan rate, v_{az} . A Gaussian beam is fully sampled at a rate of $\sim 2 / \text{FWHM}$. The maximum angular rate allowed by the detector τ is therefore

$$v_{az} = \frac{\text{FWHM}/2}{2\pi\tau}$$

or about 0.3°s^{-1} for the $30''$ beam at $250 \mu\text{m}$, and $\tau \sim 2 \text{ms}$. Mid-scan smearing in the star cameras also limits azimuthal scan speeds to about 0.1°s^{-1} . A scan rate larger than this is acceptable only for relatively small scans where star camera solutions at the turn-around are frequent enough. Low frequency ($1/f$) noise sets the largest angular mode that can be constrained to $\sim v_{az}/f_0 \sim 2^\circ$ at 0.1°s^{-1} (f_0 is the $1/f$ knee at about 50 mHz). Therefore, BLAST scans most of the time at $v_{az} \simeq 0.1^\circ \text{s}^{-1}$, occasionally going twice as fast on small ($\lesssim 0.3^\circ$ wide) maps. Azimuthal acceleration is limited to 0.1°s^{-2} , resulting in, typically, 2s for an azimuthal turn-around.

Elevation drift speeds of $10'' \text{s}^{-1}$ or elevation steps of $40''$ – $100''$ in adjacent azimuth scans provide adequate spatial sampling of the sky by the detector arrays.

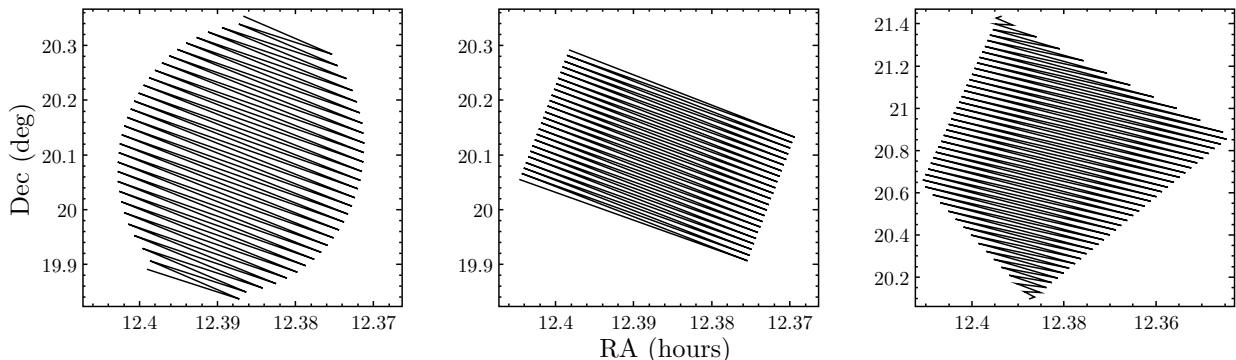


Fig. 9.— Idealized representations of BLAST’s three scan modes: from left to right a “cap”, a “box”, and a “quad”. In practice the gyroscopes are used to control the speed and orientation of each single scan, while star camera based orientation solutions at the endpoints are used to prevent gyroscope errors from accumulating.

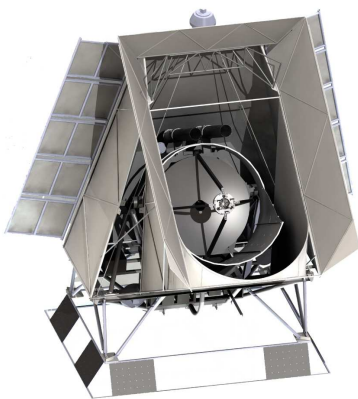


Fig. 7.— A CAD model of the gondola, showing BLAST fully assembled in the BLAST06 configuration. The electronics can cool radiatively through the triangular gaps which are visible in the sun shields. These gaps always point away from the sun in flight.

Three primary scan modes are implemented (Figure 9): “cap”, a circle centered on a target RA/Dec; “box”, a rectangle in azimuth and elevation centered on a target RA/Dec; and “quad”, an arbitrary quadrilateral specified by its four corners in RA and Dec.

8. Pointing Sensors

The primary pointing sensors for BLAST are a pair of CCD-based star cameras which provide absolute pointing, and Fiber-Optic rate Gyros that provide velocity information which can be integrated to allow interpolation of the gondola’s attitude between star camera solutions. Coarse attitude determination is provided by several additional sensors. In elevation, there is an encoder on the elevation axis, and a tilt sensor on the inner frame. In azimuth, there is a Sun sensor, a differential GPS unit, and a magnetometer. The system provides post-flight pointing reconstruction to $\lesssim 5''$ rms.

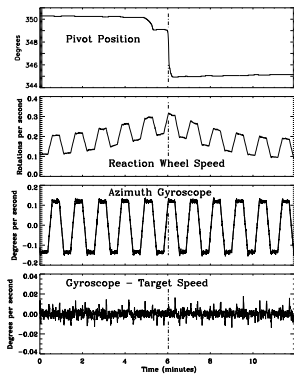


Fig. 8.— Isolation of vertical torques. All panels show data from the same 12 minute segment of the 2006 flight, during which time the telescope was executing a routine azimuthal scan. The third panel shows a trapezoidal angular velocity profile corresponding to constant angular velocity scans connected by constant angular accelerations. The third panel also includes a plot of the desired angular speeds, completely buried by the measured signal. The second panel shows that azimuthal speed is governed by accelerating and decelerating the speed of the reaction wheel. A torque at the pivot proportional to reaction wheel speed reaches threshold and overcomes the stiction in the pivot when the reaction wheel speed is near 0.3 revolutions per second. One such event is marked by the vertical dashed line in all panels. The bottom panel contains a plot of the difference between measured gyroscope signal and desired azimuthal speed. Notice that there are small spikes visible corresponding to the corners in the scan speed but that there is no azimuthal motion of the telescope itself coincident with the release of stiction in the pivot.

8.1. Star Cameras

Four primary factors drove the design of the star cameras: (i) an absolute pointing accuracy of $\sim 5''$ was required to oversample the diffraction-limited size of the $250\ \mu\text{m}$ beam; (ii) integration times (and hence efficiency) had to be short enough to avoid significant smearing at the maximum normal scan angular-velocity of the gondola (0.1°s^{-1}); (iii) the system must *always* detect stars to calibrate gyroscope drift; and (iv) the frequency of the solutions must be high enough to control the $1/f$ random walk noise in the integrated gyroscopes.

To meet these requirements, we incorporated two star cameras for redundancy, and to enable increased positional accuracy in post-flight processing. A detailed description of the cameras can be found in Rex et al. (2006), and a summary of the camera specifications is given in Table 4. Each camera uses a 100 mm Nikon lens with a 200 mm focal length to produce a $2.5^\circ \times 2.0^\circ$ FOV with $7''$ pixels. Each camera is controlled by its own PC/104, 300 MHz Celeron computer which calculates pointing solutions for the gondola at a rate of ~ 1.5 Hz. The computers command the CCD cameras via FireWire, control the focus and aperture size using stepper motors via a serial port, and regulate the temperature of the camera using a small USB DAQ module. The entire system is contained in a pressure vessel to allow the operation of the hard drives, the thermal environment, and to maintain mechanical rigidity. Since the cameras operate during the day, the dominant source of noise is from the sky background, despite the altitude of the experiment. A Nikon R60 red

filter is used to attenuate the background. In addition, a 1.2 m long cylindrical baffle is attached to the front of each camera to reduce stray-light contamination beyond 10° from the optical axis.

The pointing algorithm locates blobs in the camera image, rejecting the known bad pixels. The best fit positions of star candidates are then used by a pattern recognition algorithm to identify a unique constellation matching the observed angular separations in a star catalog (Guide Star Catalogue 1.1, see Lasker et al. 1987). The magnitude limit of the catalog is chosen manually and no brightness information for the stars is otherwise used. The algorithm is aided by an approximate pointing solution from the flight computer, required to be accurate to $\sim 5^\circ$ (see Section 8.3) to reduce the number of candidate star identifications. A visual magnitude limit of 9 was required to obtain sufficient completeness. A “Lost in Space” algorithm based on the Pyramid technique (Mortari et al. 2001) was also implemented to be used in case the approximate solution was found to be unreliable (which, ultimately, never happened during the BLAST flights).

Once the CCD object centroids are matched to stars with known coordinates (α, δ) , the pointing solution is calculated, parameterized by the celestial coordinates of the center pixel, α_0 and δ_0 , and the roll of the camera, r . A model in which the image is assumed to be a perfect gnomonic tangent-plane projection, with the tangent point at α_0 and δ_0 , is used to project each star RA and Dec into the plane of the CCD. The rms distance between the CCD and model star coordinates is then minimized using an iterative Newton solver

with respect to the three model parameters. This procedure produced pointing solutions in which the uncertainty in the position of the tangent point was $\sim 3.5''$, and the roll $\sim 200''$. A post-flight comparison of simultaneous pointing solutions from both cameras results in an rms uncertainty of $< 2''$.

8.2. Gyroscopes

Fiber-Optic rate Gyroscopes (FOG) are used to extrapolate the star camera absolute attitude, providing pointing information at each detector’s time sample. Two redundant sets of three FOGs are mechanically arranged to measure the gondola angular velocity along orthogonal axes. One of these sets uses ECORE 2000 analogue gyroscopes while the other uses DSP 3000 digital output gyroscopes from the same company¹⁷, with an angle random walk of $5'' \text{ s}^{-1/2}$ and $4'' \text{ s}^{-1/2}$, respectively. Since FOG are sensitive to magnetic fields (Bohm et al. 1982), they were wrapped in a $250 \mu\text{m}$ thick μ -metal sheet. This reduced the signal induced from the Earth’s magnetic field by a factor ~ 10 . The gyroscope assembly is temperature controlled to mitigate bias drifts. For BLAST05 both sets worked flawlessly. In BLAST06 two out of the three digital gyroscopes stopped working temporarily, possibly due to a cosmic ray interaction with the gyro electronics. A power cycle of the gyroscope itself restored function. Post-flight attitude reconstruction of the 2005 data, shows that the FOG performed at near their specified sensitivity.

¹⁷KVH Industries, Inc.

8.3. Coarse Sensors

Two distinct Sun sensors were used on BLAST for coarse azimuth determination. For BLAST03 and BLAST05 a linear CCD behind a thin slit was used. It was replaced by an array of photo-diodes arranged in a azimuthally oriented ring in BLAST06. The photo-diode Sun sensor was designed to be smaller and lighter than the CCD Sun sensor, as well as to consume significantly less power (5 W instead of 50 W).

The photo-diode Sun sensor is a small, all-in-one unit. A PC/104 embedded computer system is mounted below a dodecagonal ring. Twelve photo-diodes are mounted radially around the ring, and the ring is mounted with its axis parallel to the azimuth axis. The intensities of light incident on the photo-diode with the highest intensity and on its 2 nearest-neighbors are compared and fit to a $\cos\theta$ function to determine the azimuth relative to the Sun. The flight computer uses the time and longitude to calculate the azimuth of the Sun, hence recovering the azimuth of the gondola. The CCD Sun sensor, used during the first science flight, had a short-time, relative precision of $2'$, but an overall absolute accuracy of 5° . The photo-diode Sun sensor, used during the second science flight, had a precision of $4'$, with an absolute accuracy of 5° . Both units provide azimuthal data at > 5 Hz. In BLAST06, the sun sensor computer crashed several times, possibly due to cosmic ray interactions with the electronics.

BLAST's second coarse azimuth sensor was an ADU5 differential GPS unit¹⁸. The four required antennae were installed

on booms above the Sun shields to minimize multi-path reflections from the gondola (see Figure 6). This orientation was predicted to provide better than $10'$ rms absolute pointing. However, for BLAST05, the GPS stopped providing azimuthal solutions before the instrument reached float altitude and never recovered. For BLAST06, the GPS did not provide solutions until 110 hours after launch. It then began providing solutions and the unit operated with a precision from 0.1° to 0.2° rms. The cause of the irregular reliability of the GPS is uncertain, but may be due to a lack of thermal rigidity in the antenna mounts. The position, altitude, velocity, and time data provided by the GPS unit worked well at all times.

BLAST's third, and most reliable coarse azimuth sensor was a 3-axis, flux-gate magnetometer¹⁹ which was used to determine the gondola's attitude relative to the Earth's magnetic field. The magnetic field orientation was determined using the World Magnetic Model²⁰. Even though BLAST passed close to the magnetic pole, the model was accurate enough and the gondola pendulations small enough that the magnetometer-based pointing solution was good to 5° peak to peak in both science flights.

9. Thermal Environment

The LDB thermal environment is characterized by continuous but variable solar illumination, combined with small coupling to the atmosphere. Extensive shield-

¹⁸Magellan Navigation, Inc.

¹⁹Applied Physics, model 534.

²⁰WMM-2005, National Geospatial-Intelligence Agency (NGA).

ing is used to regulate the temperature of the instrument. Following the design of BOOMERANG (Crill et al. 2003), BLAST is surrounded by shields comprised of 24 μm thick aluminized Mylar applied to 2.5 cm thick polystyrene open-celled foam. The Mylar side faces out on all surfaces which may be exposed to the Sun. While bare aluminum surfaces can be expected to reach temperatures in excess of 130°C in the LDB float environment, Sun-facing aluminized Mylar surfaces reach temperatures of around 45°C due to their high ratio of thermal IR emissivity to visible light absorptivity. For telescope azimuth ranges of $\pm 60^\circ$ from anti-Sun, the shielding blocks direct radiation from reaching the optics and all electronics, except for the pivot motor controller and Sun sensor. The actual angles of Sun avoidance have a weak dependence on the elevation of the telescope.

The majority of the electronics dissipate their heat radiatively. A high IR emissivity is achieved by painting electronics enclosures with white paint. Painting white the interiors of boxes aids in radiative transfer between the electronics and the box. This is effective for all boxes, except for the detector readout electronics boxes, each of which dissipate about 100 W. To cool these boxes, emissive vertical plates were installed between each card to couple heat from the electronics to the top and bottom walls of the boxes. A closed-cycle fluid cooling loop was used to distribute the heat to the gondola frame.

The thermal strategy was effective in keeping the temperatures of essentially all electronics well within their operational range. For BLAST06, the shield, added to

keep the Sun from illuminating the secondary mirror, reflected solar radiation back onto the pivot motor controller. This increased the average temperature of the pivot by up to 20°C compared to what was experienced in BLAST05. As a result, two non-essential observations were shortened when the motor controller temperature exceeded 62.5°C.

For the 2006 flight, the primary mirror was thermally isolated from the inner frame with G10 spacers and a several layer of Mylar Super-insulation was added in the gap between the mirror and the frame. This stabilized the in-flight temperature that had a diurnal excursion of about 3°C.

Please, see Table 5 and Figure 10 for a list of temperatures achieved during the various BLAST flights.

10. Power System

Solar panels provide power to the flight electronics. They are mounted on the support structure for the Sun shields, at the back of the telescope, and are unfolded sideways at port and starboard (Figure 6). The panels face the Sun from only one side and are radiatively cooled to the sky from the other side.

During normal operation, BLAST requires 540 W, divided between two completely isolated systems: the receiver, and the rest of the gondola. During line-of-sight operations, an additional 160 W are required to power the transmitters. Power is provided by the solar power system²¹

²¹MEER Instruments, Palomar Mountain, CA, <http://www.meer.com/> and SunCat Solar, Phoenix, AZ.

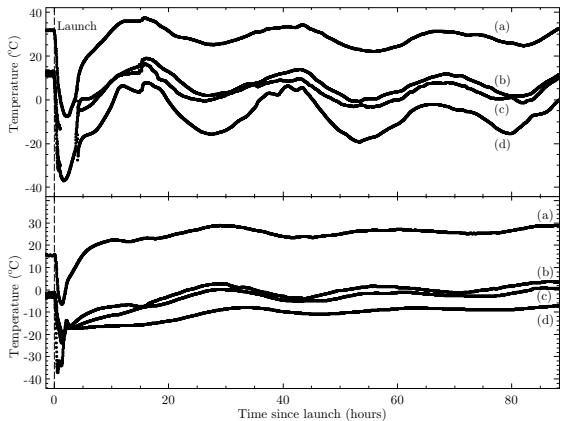


Fig. 10.— Temperatures during the Northern Hemisphere (top panel) and antarctic (bottom) flights: Several gondola temperatures are plotted for the period starting just before launch and extending through the first few days from both science flights. Dramatic cooling in the troposphere, reheating in the stratosphere and diurnal variations due to variation of the solar elevation angle are visible in all traces. The curves are a: the pressure vessel containing the data acquisition computers, b: the gondola inner frame, c: the elevation axis motor and d: the primary mirror. The temperature difference between high power consumption electronics (a) and more passive components (b and c) is only slightly larger at float than it is on the ground. The primary mirror has the best geometry for cooling radiatively and therefore attains the coldest temperature. Notice the relatively large variations in the primary mirror temperature in the 2005 flight which caused us to recognize the need for in-flight focussing capability.

which charges NiMH batteries²². The arrays provide 1250 W for normal incidence at float. The arrays are thus able to provide full power to the experiment up to a Sun-array angle of $> 60^\circ$. The batteries are essentially only used during launch and ascent.

As a NiMH battery reaches its top-off voltage, its charge efficiency decreases, leading to heating of the battery. Additionally, the topoff voltage of NiMH batteries decreases with increased temperature. This combination can lead to thermal runaway if the batteries are charged with a fixed top-off voltage. For BLAST, the charge controllers were modified to allow the flight computer to reduce the top-off voltage as the battery temperature increases, permitting full battery charge without thermal runaway.

11. Flight Planning

BLAST is designed to target multiple regions with a variety of science goals. Unlike a ground-based telescope at a fixed geographic location, the visibility constraints for BLAST change in real-time. The instantaneous region of the sky that is available varies with time, and location of the payload. Finally, the launch date and time are highly uncertain; for every launch opportunity, a new flight plan must therefore be created.

BLAST functions autonomously using schedule files that consist of a sequential list of observations or actions as a function of the Local Sidereal Time. This system is robust against temporary system failures because the telescope only needs to know

²²Cobasys Model 9500.

the current time and location to resume operation upon recovery. Using a local sidereal clock rather than a clock fixed in some time zone, it is possible to account for purely astronomical visibility constraints using a static description, such as the RA of the Sun and of the astronomical targets. It has the disadvantage that the duration the telescope spends on a given observation will vary depending on telescope longitudinal drifts.

A schedule file generator was developed to interpret a high-level description of the desired scientific observations, (e.g. map a circular region centered at a given RA and DEC with a given radius). It also accounts for a number of parameters: the launch date and time, projected duration of flight, the start longitude and latitude, a guess for the termination longitude, a latitude range for the payload, and the position of the Sun and the Moon. With this information the scheduler generates an optimized list of consecutive actions. At each instant, observations that are possible under the current visibility constraints are scheduled in order of priority. At regular intervals, calibration observations are assigned maximum priority, so that sensitivity, beam shape, and pointing variations may be tracked throughout the flight. Once a schedule file is generated, a simple model for the power usage of the system, and the charge rate of the solar panels as a function of Sun incidence angle, is used to calculate the available battery charge over time. The schedule is modified if this model indicates that the batteries will have less than 50% of the total charge capacity at any point in the flight. Schedules are then tested using a simulator that mimics

the scanning motion of the telescope to determine the coverage (effective integration time across the maps), and cross-linking among each of the maps for a given flight trajectory.

For every launch opportunity, six schedule files are generated. The latitude of the gondola can change by as much as $\sim 15^\circ$ during a flight, hence three different schedules are created in latitude bands that are 6° wide, with 1° of overlap. The gondola uses the GPS to decide which schedule file to use. Two sets of these three schedules are made: the first set assumes the instrument is working with the target sensitivities; the second assumes degradations of the telescope beam size by a factor of $\sqrt{2}$, and sensitivity by a factor of 2. At the beginning of the flight, the sensitivities are estimated from scans across calibrators. Based on this information the ground station team can decide which of the two sets of schedule files the instrument should use, and switch between the two using a single command, if required.

12. Pointing Reconstruction

Post-flight pointing reconstruction estimates the rotation (attitude) of the gondola with respect to the celestial sphere as a function of time, providing RA, Dec, and rotation angle information at each sample of the detectors. The star camera provides absolute attitude on an unevenly sampled time grid (~ 1.5 s), with an accuracy of $< 2''$ rms. Each solution is sampled at a known phase with respect to the detectors. The detector and gyroscope sampling are synchronized; therefore, the integration of the gyroscopes gives one estimate of the gondola attitude. The star camera

is used to correct the random walk drift induced by the integrated gyroscope noise and as an estimate of the integration constant. BLAST implements a Kalman filter approach to estimate the attitude, expressed as the state quaternion $q(t)$, a 4 dimensional quantity describing the solid body rotation of the gondola. The non-linear state model representing the gondola is defined as

$$\begin{cases} \vec{b}_{n+1} = \vec{b}_n + \vec{w}_{bn} \\ q_{n+1} = \left(\begin{array}{c} 1 \\ \frac{1}{2} (\vec{\omega}_n + \vec{b}_n + \vec{w}_{\omega n}) \Delta T \end{array} \right) q_n \end{cases} \quad (1)$$

where $\vec{\omega}_n$ is the gyro angular velocity with $\vec{w}_{\omega n}$ its noise, \vec{b}_n is the gyro bias, \vec{w}_{bn} is the filter process noise and ΔT is the time resolution of the system (10 ms). The filter is run forward and backward in time and the two solutions are weighed together, using the Kalman covariance matrix output from the filter as the weight. Using just one star camera and the digital gyros, the final averaged attitude is better than 5" rms; one example is shown in Figure 11 using data from the BLAST05 flight. The achieved precision is sufficient for BLAST beam sizes, but can be improved once the second set of gyroscopes and the additional star camera are included in the solution. An improvement of $\sqrt{2}$ to 2 better can be reasonably expected. The pointing solution is referenced to the star camera reference frame and needs to be rotated into the submillimeter array coordinate frame. Bright optical and submillimeter point sources are used to evaluate the rotation quaternion Q to apply.

The correction Q is ideally static, but, in practice, was found to be a weak function of time. As shown in Figure 6, the star

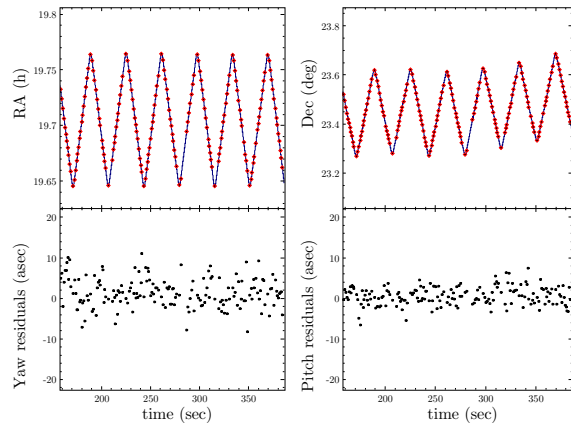


Fig. 11.— An example of pointing reconstruction from the BLAST05 data. In the top plots, the solid blue lines represent the reconstructed pointing solution obtained integrating one set of gyroscopes onto one of the two star cameras. Dots represent the positions reported by the other star camera, which is not used in the solution. The bottom panels show the residuals as yaw ($\sim \Delta RA * \cos(\text{Dec})$) and pitch (coincident with Dec in this particular case). The yaw residuals are slightly wider, since the telescope scans in azimuth, which is close to RA at the BLAST05 latitudes. The projection of the gondola angular velocity along the yaw axis is always larger than the pitch axis for the elevation range of the telescope (25° – 60°), and hence the star centroids in star camera images have larger measurement errors in that direction. The overall error of the pointing solution can be obtained by summing in quadrature the standard deviations of the residuals, yielding $\simeq 4.2''$ rms. Improvements to this result are discussed in Section 12

cameras are mounted at the top of the inner frame, and a structural deformation of the frame can modify the relative orientation between the cameras and the submillimeter beam. Therefore, several pointing calibrators are observed each time the geometry of the scan changes. This effect can be as large as 35'' and has an 80% correlation with the elevation, and a 25% correlation with the temperature of inner frame. Although it is possible to model the effect based on the gondola thermometry and attitude, Q is such a weak function of time that this was found unnecessary.

13. Conclusion

BLAST is a unique instrument designed to probe the local and high- z Universe at short submillimeter wavelengths. Over the course of two science flights, BLAST has addressed a broad range of Galactic and extragalactic topics. The balloon environment requires a novel combination of ground and satellite technology and techniques. This paper is intended to serve as a reference for a suite of science papers from the BLAST05 and BLAST06 flights.

The BLAST collaboration acknowledges the support of NASA through grant numbers NAG5-12785, NAG5-13301 and NNGO-6GI11G, the Canadian Space Agency (CSA), the UK Particle Physics & Astronomy Research Council (PPARC), Canada's Natural Sciences and Engineering Research Council (NSERC), the Canada Foundation for Innovation, the Ontario Innovation Trust, the Puerto Rico Space Grant Consortium, the Fondo Institucional para la Investigacion of the University of Puerto Rico, and the National Science

Foundation Office of Polar Programs; C. B. Netterfield also acknowledges support from the Canadian Institute for Advanced Research. L. Olmi would like to acknowledge Pietro Bolli for his help with Physical Optics simulations during the testing phase of the BLAST06 telescope. We would also like to thank the Columbia Scientific Balloon Facility (CSBF) staff for their outstanding work, the Precision Machining Group at Lawrence Livermore Laboratory, the support received from Amec in the design and construction of the gondola, Daniele Mortari for helpful discussions in the development of the Pyramid code, Dan Swetz for building the Fourier transform spectrometer, and Luke Bruneaux, Kyle Lepage, Danica Marsden, Vjera Miovic, and James Watt for their contribution to the project.

REFERENCES

- Ade, P. A. R., Pisano, G., Tucker, C., & Weaver, S. 2006, in Presented at the Society of Photo-Optical Instrumentation Engineers (SPIE) Conference, Vol. 6275, Millimeter and Submillimeter Detectors and Instrumentation for Astronomy III. Edited by Zmuidzinas, Jonas; Holland, Wayne S.; Withington, Stafford; Duncan, William D.. Proceedings of the SPIE, Volume 6275, pp. 62750U (2006).
- Bock, J. J., Delcastillo, H. M., Turner, A. D., Beeman, J. W., Lange, A. E., & Mauskopf, P. D. 1996, in ESA SP-388: Submillimetre and Far-Infrared Space Instrumentation, ed. E. J. Rolfe & G. Pilbratt, 119–+

- Bohm, K., Petermann, K., & Weidel, E. 1982, *Optics Letters*, 7, 180
- Chattopadhyay, G., Glenn, J., Bock, J. J., Rownd, B. K., Caldwell, M., & 2003, M. J. G. 2003, *IEEE Trans. Micro. T. Tech*
- Crill, B. P., Ade, P. A. R., Artusa, D. R., Bhatia, R. S., Bock, J. J., Boscaleri, A., Cardoni, P., Church, S. E., Coble, K., de Bernardis, P., de Troia, G., Farese, P., Ganga, K. M., Giacometti, M., Haynes, C. V., Hivon, E., Hristov, V. V., Iacoangeli, A., Jones, W. C., Lange, A. E., Martinis, L., Masi, S., Mason, P. V., Mauskopf, P. D., Miglio, L., Montroy, T., Netterfield, C. B., Paine, C. G., Pascale, E., Piacentini, F., Polenta, G., Pongetti, F., Romeo, G., Ruhl, J. E., Scaramuzzi, F., Sforna, D., & Turner, A. D. 2003, *ApJS*, 148, 527
- Devlin, M. J., Ade, P. A. R., Aretxaga, I., Bock, J. J., Chung, J., Chapin, E., Dicker, S. R., Griffin, M., Gundersen, J., Halpern, M., Hargrave, P., Hughes, D., Klein, J., Marsden, G., Martin, P., Mauskopf, P. D., Netterfield, B., Olmi, L., Pascale, E., Rex, M., Scott, D., Semisch, C., Truch, M., Tucker, C., Tucker, G., Turner, A. D., & Weibe, D. 2004, in Presented at the Society of Photo-Optical Instrumentation Engineers (SPIE) Conference, Vol. 5498, Millimeter and Submillimeter Detectors for Astronomy II. Edited by Jonas Zmuidzinas, Wayne S. Holland and Stafford Withington Proceedings of the SPIE, Volume 5498, pp. 42-54 (2004)., ed. C. M. Bradford, P. A. R. Ade, J. E. Aguirre, J. J. Bock, M. Dragovan, L. Duband, L. Earle, J. Glenn, H. Matsuhara, B. J. Naylor, H. T. Nguyen, M. Yun, & J. Zmuidzinas, 42–54
- Griffin, M. J., Bock, J. J., & Gear, W. K. 2002, *Appl. Opt.*, 41, 6543
- Griffin, M. J., Swinyard, B. M., & Vigroux, L. G. 2003, in Presented at the Society of Photo-Optical Instrumentation Engineers (SPIE) Conference, Vol. 4850, IR Space Telescopes and Instruments. Edited by John C. Mather . Proceedings of the SPIE, Volume 4850, pp. 686-697 (2003)., ed. J. C. Mather, 686–697
- Hargrave, P., Waskett, T., Lim, T., & Swinyard, B. 2006, in Presented at the Society of Photo-Optical Instrumentation Engineers (SPIE) Conference, Vol. 6275, Millimeter and Submillimeter Detectors and Instrumentation for Astronomy III. Edited by Zmuidzinas, Jonas; Holland, Wayne S.; Withington, Stafford; Duncan, William D.. Proceedings of the SPIE, Volume 6275, pp. 627514 (2006).
- Holland, W., MacIntosh, M., Fairley, A., Kelly, D., Montgomery, D., Gostick, D., Atad-Ettdgui, E., Ellis, M., Robson, I., Hollister, M., Woodcraft, A., Ade, P., Walker, I., Irwin, K., Hilton, G., Duncan, W., Reintsema, C., Walton, A., Parkes, W., Dunare, C., Fich, M., Kyrcia, J., Halpern, M., Scott, D., Gibb, A., Molnar, J., Chapin, E., Bintley, D., Craig, S., Chylek, T., Jenness, T., Economou, F., & Davis, G. 2006, in Presented at the Society of Photo-Optical Instrumentation Engineers (SPIE) Conference, Vol. 6275, Millimeter and Submillimeter Detectors and Instrumentation for Astronomy III. Edited by

- Zmuidzinas, Jonas; Holland, Wayne S.; Withington, Stafford; Duncan, William D.. Proceedings of the SPIE, Volume 6275, pp. 62751E (2006).
- Hughes, D. H., Aretxaga, I., Chapin, E. L., Gaztañaga, E., Dunlop, J. S., Devlin, M. J., Halpern, M., Gundersen, J., Klein, J., Netterfield, C. B., Olmi, L., Scott, D., & Tucker, G. 2002, MNRAS, 335, 871
- Lamarre, J. M., Giard, M., Pointecouteau, E., Bernard, J. P., Serra, G., Pajot, F., Désert, F. X., Ristorcelli, I., Torre, J. P., Church, S., Coron, N., Puget, J. L., & Bock, J. J. 1998, ApJ, 507, L5
- Lasker, B. M., Jenkner, H., & Russell, J. L. 1987, NASA STI/Recon Technical Report N, 88, 30547
- Mather, J. C. 1984, Appl. Opt., 23, 584
- Mortari, D., Junkins, J. L., & Samaan, M. A. 2001, Lost-in-Space Pyramid Algorithm for Robust Star Pattern Recognition, AAS Paper 01-004 of the 22th Annual AAS Rocky Mountain Guidance and Control
- Olmi, L. 2001, Int. J. of Infrared and Millim. Waves, 22, 791
- Olmi, L. 2002, in Presented at the Society of Photo-Optical Instrumentation Engineers (SPIE) Conference, Vol. 4849, Highly Innovative Space Telescope Concepts Edited by Howard A. MacEwen. Proceedings of the SPIE, Volume 4849, pp. 245-256 2002., ed. H. A. MacEwen, 245-256
- . 2007, Applied Optics, Accepted for publication, 791
- Patanchon, G. et al. 2007, ApJ, submitted
- Rex, M., Chapin, E., Devlin, M. J., Gundersen, J., Klein, J., Pascale, E., & Wiebe, D. 2006, in Presented at the Society of Photo-Optical Instrumentation Engineers (SPIE) Conference, Vol. 6269, Ground-based and Airborne Instrumentation for Astronomy. Edited by McLean, Ian S.; Iye, Masanori. Proceedings of the SPIE, Volume 6269, pp. 62693H (2006).
- Rownd, B., Bock, J. J., Chattopadhyay, G., Glenn, J., & Griffin, M. J. 2003, in Presented at the Society of Photo-Optical Instrumentation Engineers (SPIE) Conference, Vol. 4855, Millimeter and Submillimeter Detectors for Astronomy. Edited by Phillips, Thomas G.; Zmuidzinas, Jonas. Proceedings of the SPIE, Volume 4855, pp. 510-519 (2003)., ed. T. G. Phillips & J. Zmuidzinas, 510-519
- Truch, M. et al. 2007, ApJ, submitted
- Turner, A. D., Bock, J. J., Beeman, J. W., Glenn, J., Hargrave, P. C., Hristov, V. V., Nguyen, H. T., Rahman, F., Sethuraman, S., & Woodcraft, A. L. 2001, Appl. Opt., 40, 4921

This 2-column preprint was prepared with the AAS L^AT_EX macros v5.2.

TABLE 1
BLAST OPTICS DESIGN SUMMARY.

Element	BLAST05	BLAST06
Mirror Diameter	2 m	1.8 m
Focal Length	10 m	9 m
Field Taper	-15 db	-7.5 db
Obscuration	14%	7%
FWHM $250\mu m$	40''	30''
FWHM $350\mu m$	58''	42''
FWHM $500\mu m$	75''	60''
Overall transmission	—— 30% ——	

NOTE.—The BLAST05 instrument used a larger mirror which was under-illuminated. In order to maintain the point-source detectability, the BLAST06 telescope was more aggressively illuminated.

TABLE 2
SUMMARY OF RELEVANT DETECTOR CHARACTERISTICS.

	250 μm	350 μm	500 μm
Light detectors	139	88	43
Dark pixels	2	2	2
Resistors	1	1	1
Thermistors	2	2	2
G (pW/K)	880	640	480
Δ (K)		50	
R_0 (M Ω)		55	
R_L (M Ω)		7 + 7	
τ (ms)		2	
Temperature (mK)		270	
NEP (W Hz $^{-1/2}$)		3×10^{-17}	

NOTE.—Bolometer parameters are given for a typical array pixel. Δ and R_0 define the bolometric model, $R(T) = R_0 e^{\sqrt{\Delta/T}}$, while the optical time constant, τ , and the thermal conductance, G , define its thermal behavior. The NEP is computed at 1 Hz.

TABLE 3
WEIGHTS OF THE MAIN COMPONENTS ON THE PAYLOAD.

Component	Weight (kg)
Inner Frame	705
Frame	120
Mirror	115
Cryostat (empty)	215
Electronics	65
Cryogenics	85
Outer Frame	1100
Batteries	80
Solar Panels	30
Electronics	110
Sun Shields	195
Frame	195
CSBF Hardware & Electronics	215
Total Weight at Launch	2020

NOTE.—Bold face values refer to the BLAST06 configuration and include the items shown here as well as all the other elements on the gondola. The total weight at launch was measured at the hook of the launch vehicle before take-off.

TABLE 4
SPECIFICATIONS OF THE TWO CCD STAR CAMERAS

Camera	PMI 1401	Retiga EXi
Pixels	1312×1024	1360×1036
Pixel Size	$6.8 \mu\text{m} \times 6.8 \mu\text{m}$	$6.45 \mu\text{m} \times 6.45 \mu\text{m}$
Dynamic range	14 bit	12 bit
Well Depth	$45,000 e^-$	$18,000 e^-$

NOTE.—The cameras are manufactured by QImaging (<http://www.qimaging.com/>). Though both star cameras are nearly identical, the PMI 1401 has deeper pixel wells. It was also found to have a lower measured optical efficiency, significant readout noise and gain variations across the chip compared to the Retiga EXi. However, despite requiring longer integration times to reach a given s.n.r., the greater dynamic range of the PMI 1401 afforded by the extra well depth enabled it to function in backgrounds 1.6 times larger than for the Retiga EXi. The shape of the spectral response for each camera is similar with peaks in the range 400 nm – 850 nm.

TABLE 5
BLAST TEMPERATURES (°C).

	BLAST03		BLAST05		BLAST06		Model
	Trop	Diurnal	Trop	Diurnal	Trop	Diurnal	
ACS 5V DCDC ^a	25	51 to 23	15	62 to 46	3.6	41 to 36	...
ACS Case ^b	-30	21 to 1	-21	16 to 10	28 to 13
PV Case ^c	-21	21 to 13	-21	17 to 12	18 to 4
PV Air	-5	26 to 1	-7	35 to 24	-6	24 to 29	...
Preamplifier Case ^d	-20	10 to -10	...	31 to 19	-5	25 to 21	25 to 19
Inner Frame	-16	-2 to -27	-22	14 to -2	-32	-2 to -5	...
Batteries ^f	10	17 to 10	-3	21 to 10	-6	19 to 17	16 to 0
Solar Panels ^g	-30	66 to 5	-29	79 to 58	85
Mylar Shields	-30	17 to -55	-34	18 to -4	-38	20 to 10 ^h	...
Primary Mirror	-24	-8 to -38	...	8 to -15	-17	-6 to -9	-25 to -10
Secondary Mirror	-33	0 to -70	-26	-13 to -16 ⁱ	...
Pivot	-33	15 to -50	-38	20 to -5	-35	57 to 36 ^j	...
Outer Frame ^k	-11	-1.4 to -37	-30	5 to -13	-24	2 to -3	25 to -5
Star Camera	-11	15 to 1	-12	6 to 1	18 to 5
Sun Sensor ^l	0	31	-23	43 to 30

NOTE.—BLAST temperatures in the three flights, and as predicted by a Thermal Desktop (<http://www.thermaldesktop.com/>) model for BLAST06. The model predicted larger diurnal variations than observed, partially because BLAST06 followed a very southerly track, where the sun elevation varied less than the simulation's track. The *Trop* column gives the minimum temperature the component reached during ascent through the Tropopause. The *Diurnal* column gives the daily range of temperatures. In some cases, there was slowly increasing temperature over and above the diurnal variation, due to UV degradation of the Mylar shields.

^aThe inside of the case was painted white before BLAST06.

^bPartially painted white.

^cPainted white.

^dPainted white + cooling loop.

^fPackaged in a foam box.

^gThe model neglects current draw.

^hIncreased by 20°C over 12 days.

ⁱIncreased by 5°C over 12 days.

^jIncreased by 4°C over 12 days

^kMeasured at the lock motor near the elevation bearing.

^lWith cooling pump to heat exchanger.